The Journal of Membrane Biology (2018) 251:345–356
https://doi.org/10.1007/s00232-018-0026-y

Computed Free Energies of Peptide Insertion into Bilayers are Independent of Computational Method

James C. Gumbart[1] · Martin B. Ulmschneider[2] · Anthony Hazel[1] · Stephen H. White[3] · Jakob P. Ulmschneider[4]

Received: 29 September 2017 / Accepted: 27 February 2018 / Published online: 8 March 2018

Abstract
We show that the free energy of inserting hydrophobic peptides into lipid bilayer membranes from surface-aligned to transmembrane inserted states can be reliably calculated using atomistic models. We use two entirely different computational methods: high temperature spontaneous peptide insertion calculations as well as umbrella sampling potential-of-mean-force (PMF) calculations, both yielding the same energetic profiles. The insertion free energies were calculated using two different protein and lipid force fields (OPLS protein/united-atom lipids and CHARMM36 protein/all-atom lipids) and found to be independent of the simulation parameters. In addition, the free energy of insertion is found to be independent of temperature for both force fields. However, we find major difference in the partitioning kinetics between OPLS and CHARMM36, likely due to the difference in roughness of the underlying free energy surfaces. Our results demonstrate not only a reliable method to calculate insertion free energies for peptides, but also represent a rare case where equilibrium simulations and PMF calculations can be directly compared.

Keywords Peptide partitioning · Transfer free energy · Translocon · Membrane · Molecular dynamics

Introduction

Membrane-protein insertion into a lipid bilayer typically occurs via one of the two pathways. The simplest is direct partitioning from the aqueous environment, a pathway taken predominantly by single-transmembrane (TM)-spanning helices such as pore-forming toxins (Schlamadinger et al. 2012) and antimicrobial peptides (Bechinger 1997; Sato and Feix 2006; Ulmschneider 2017; Upadhyay et al. 2015; Wang et al. 2016) due to their opportunistic and adventitious nature. For natively synthesized membrane proteins, the most common pathway in all organisms relies on the protein translocon, itself a membrane protein that provides a route to the hydrophobic core of the bilayer through its lateral gate (Frauenfeld et al. 2011; Park et al. 2014; van den Berg et al. 2004).

Although both pathways lead to the same fate for a protein, stable incorporation in the membrane, differences in energetics of the initial states (Gumbart et al. 2011b) and kinetics of the processes (Gumbart et al. 2013; Zhang and Miller 2012a) can lead to one pathway being favored over the other. Thus, a complete biophysical description of these pathways will ultimately depend on a quantitative measure of the interactions between the inserting protein and its three possible environments: water, membrane, and translocon. While experiments have been quite successful at probing the translocon-mediated pathway (Hessa et al. 2005; Hessa et al. 2007), direct partitioning has proven more difficult to systematically study due to the aggregation tendencies of many hydrophobic peptides (Wimley and White 2000).

Computer simulations present an appealing alternative to experiments for understanding membrane-protein insertion, because all facets of the process being simulated are available for detailed scrutiny. Nonetheless, their utility is heavily dependent on the accessible time scales and the accuracy of the underlying force fields. The former concern can be

✉ James C. Gumbart
gumbart@physics.gatech.edu

✉ Jakob P. Ulmschneider
jakob@sjtu.edu.cn

[1] School of Physics, Georgia Tech, Atlanta, GA, USA

[2] Department of Chemistry, King's College, London SE1 1DB, UK

[3] Department of Physiology & Biophysics, University of California at Irvine, Irvine, CA, USA

[4] Department of Physics and the Institute of Natural Sciences, Shanghai Jiao Tong University, Shanghai 200240, China

met either through increasing the computational efficiency of simulations, e.g., by using the latest supercomputers such as Anton (Hu et al. 2016), or through enhanced sampling methods that permit calculation of free energies from biased simulations, e.g., umbrella sampling. Despite apparent successes of both approaches (Gumbart et al. 2013; Horn et al. 2013), recent work has indicated sampling difficulties for membrane-peptide interactions may have been drastically underestimated previously (Neale et al. 2011). The latter concern, that of the force fields, also represents an unsettled issue, in which different approaches in development have led to apparently different outcomes (Piggot et al. 2012).

Free energies of insertion for individual amino acids have been determined experimentally using an approach where insertion occurs via Sec61 (Hessa et al. 2005; Hessa et al. 2007) as well as an approach in which a guest residue is incorporated in OmpLA, a β-barrel membrane protein that can spontaneously fold and insert (Moon and Fleming 2011). A number of simulation studies have followed these approaches, focusing on side-chain analogs (Johansson and Lindahl 2008; MacCallum et al. 2007) or single amino acids embedded in proteins (Dorairaj and Allen 2007; Gumbart et al. 2011b; Gumbart and Roux 2012). Although challenging due to aggregation tendencies as noted above, insertion energies for small α-helical peptides have been measured experimentally in limited cases, e.g., for toxins (Ladokhin and White 2004), antimicrobial peptides (Ladokhin and White 1999), and designed peptides (Wimley and White 2000), as well as computationally (Babakhani et al. 2008; Irudayam et al. 2013; Lyu et al. 2017; Sandoval-Perez et al. 2017; Yeh et al. 2008).

In order to evaluate the consistency of various approaches and force fields to understanding lipid-protein interactions, we have calculated the energetics and kinetics of membrane partitioning for short polyleucine helices, denoted L*n* ($n = 5$–10). We used two completely unrelated protein (OPLS and CHARMM36) and lipid (united-atom and all-atom) force fields, as well as both long equilibrium simulations and potential-of-mean-force calculations to resolve the energetic landscape of the partitioning process. The results are found to be almost uniformly in quantitative agreement across methods and force fields. The only exception is in the rate of transitions between states, likely due to the simplified (united-atom) lipid model used in the OPLS force field. Our results demonstrate that peptide partitioning simulations are reliable and that the energetics of partitioning depend little on force field parameters and simulation techniques; however, the kinetics, in particular the diffusivity, does depend on the lipid model used.

Methods

Equilibrium Molecular Dynamics (MD)

Peptide sequences of the form ac-L_n-nme (L*n*, $n = 5$–10) were constructed and embedded into the water phase of a box containing a preformed POPC (palmitoyloleoylphosphocholine) lipid bilayer. The initial conformation was an ideal α-helix, placed 10 Å from the bilayer surface. Equilibrium simulations at 50, 120, and 160 °C were run on the Anton 1 machine at Pittsburgh Supercomputing Center (Shaw et al. 2009) and analyzed with VMD (Humphrey et al. 1996), while all others were performed and analyzed using Gromacs version 4.5 (http://www.gromacs.org) (Berendsen et al. 1995) and hippo beta (http://www.biowerkzeug.com/). The CHARMM36 protein (Best et al. 2012) and lipid (Klauda et al. 2010) force fields were used along with TIP3P for water (Jorgensen et al. 1983) for all equilibrium simulations.

For Gromacs simulations, electrostatic interactions were computed using the particle-mesh Ewald method (PME); a cutoff of 10 Å was used for van der Waals interactions. Bonds involving hydrogen atoms were restrained using LINCS (Hess et al. 1997). Simulations were run with a 2-fs integration time-step. All simulations were performed in the NPT ensemble, with no additional applied surface tension. Water, lipids, and the protein were each coupled separately to a heat bath with time constant $\tau_T = 0.1$ ps using weak temperature coupling (Bussi et al. 2007); atmospheric pressure of 1 bar was maintained using weak semi-isotropic pressure coupling with compressibility $\kappa_z = \kappa_{xy} = 4.6 \times 10^{-5}$ bar^{-1} and time constant $\tau_P = 1$ ps (Berendsen et al. 1984).

In Anton simulations, a 2.5-fs time step was used. Temperature and pressure control were enabled through application of the Multigrator approach (Lippert et al. 2013) using a semi-isotropic Martyna–Tuckerman–Klein barostat (Martyna et al. 1994) and Nosé–Hoover thermostat (Hoover 1985; Martyna et al. 1992). Short-range and long-range nonbonded interactions were updated every time step and every three time steps, respectively. For all simulations on Anton, the cutoff was automatically chosen to be around 13–14 Å.

The insertion propensity p_{TM} of each peptide was calculated as the probability of the peptide being in the TM state. To distinguish the TM state from the S state, a criterion of $z < 8$ Å and $\theta < 50°$ was found to be optimal. The free energy of S → TM partitioning was then calculated as $\Delta G_{S \to TM} = \; + kT \ln(1/p_{TM} - 1)$. Sufficient transition events were captured by using elevated temperatures. No loss of helical structure occurred even at temperatures as high 150 °C, for any sequence tested. We used helical restraints for $T > 150$ °C.

Free-Energy Calculations

All simulations used for potential-of-mean-force (PMF) calculations, denoted "US" in Table 1, were run with NAMD (Phillips et al. 2005). Simulations were run using either the CHARMM36 or the OPLS force field. In the case of OPLS, protein parameters were taken from the CHARMM-formatted file par_opls_aa.inp (Jorgensen et al. 1996), distributed along with the CHARMM force field, while lipid parameters were taken from Ulmschneider et al. (2010b). In all cases, the TIP3P force field for water was used (Jorgensen et al. 1983).

For PMF calculations run using the CHARMM36 force field, a cutoff of 12 Å was used for short-range non-bonded interactions with a force-based switching function starting at 10 Å. For simulations with the OPLS force field, a cutoff of 10 Å was used for short-range non-bonded interactions with a potential-based switching function starting at 8 Å; interactions between atoms separated by three bonds ("1–4 interactions") were scaled by 0.5. Lennard–Jones interactions were calculated using an arithmetic combination rule for CHARMM36 and a geometric combination rule for OPLS. In all simulations in this section, a 2-fs time step was used with long-range electrostatics calculated using PME every other time step. Temperature was controlled with a Langevin thermostat with a damping constant of 0.1 ps^{-1}; pressure was maintained at 1 atm separately in the *xy* and *z* dimensions using a Langevin piston (Feller et al. 1995).

PMFs were calculated using umbrella sampling with replica exchange (REMD-US), which permits swapping periodically between neighboring windows to enhance conformational-space sampling (Sugita et al. 2000), as implemented in NAMD. Two reaction coordinates were used. The first is the position of the peptide helix along the membrane normal *z*, which was divided into 12 windows spaced every 1.5 Å from −0.5 to 16.0 Å; *z* is calculated as the distance between the centers-of-mass of the peptide backbone and of the phosphorus atoms of the lipids. The angle of the peptide's helical axis with the membrane normal is the second coordinate, with 8 windows spaced evenly over 90° used. Thus, for 2D REMD-US, 96 windows were needed. After a 1-ns equilibration per window, 31 ns/window was run for most PMFs, making the typical net simulation time 3 µs/PMF (see Table 1).

Diffusivity Calculations

Diffusivity was calculated through use of a generalized Langevin approach (Gaalswyk et al. 2016). For each window from the REMD-US simulations, an additional 2-ns simulation was run in which the L8 peptide was harmonically restrained to that window's center, (z_i, θ_i). From this

Table 1 List of all simulations performed

Sequence	Force field	Simulation type	T [°C]	Length [µs]	$\Delta G_{S\rightarrow TM}$ [kcal/mol]
L8	C36	MD	50	10.0	−0.98 ± 0.18
L8	C36	MD	120	7.2	−0.79 ± 0.43
L8	C36	MD	150	5.0	−0.54 ± 0.43
L8	C36	MD	160	2.5	−1.08 ± 0.09
L8	C36	MD [R]	180	5.0	−0.92 ± 0.30
L8	C36	MD [R]	210	5.0	−1.14 ± 0.19
L8	C36	US [R]	50	3.8	−2.86 ± 0.07
L8	C36	US [R]	120	3.0	−1.27 ± 0.14
L8	C36	US [R,x2]	120	1.0	−1.48 ± 0.14
L8	C36	US [R]	160	3.0	−1.38 ± 0.12
L8	OPLS	US [R]	50	3.0	−1.27 ± 0.18
L8	OPLS	US [R]	120	3.0	−1.00 ± 0.18
L8	OPLS	US [R]	160	3.0	−1.61 ± 0.03
L5	C36	MD	150	2.1	3.29 ± 0.20
L6	C36	MD	150	2.2	1.44 ± 0.26
L7	C36	MD	120	3.0	0.61 ± 0.28
L7	C36	MD	150	2.2	0.57 ± 0.48
L7	C36	MD	160	2.4	0.99 ± 0.18
L9	C36	MD [R]	210	2.0	−2.03 ± 0.39
L10	C36	MD [R]	210	2.8	−2.65 ± 0.59

C36 refers to CHARMM36 force field for both protein and lipids; OPLS refers to that force field for protein and the united-atom lipids. Under simulation type, MD is purely equilibrium, while US refers to replica-exchange umbrella sampling. "[R]" indicates the use of helical restraints on the peptide. Error bars are derived from block averaging over five blocks of equal length. The aggregate simulation time is over 71 µs

simulation, the velocity autocorrelation function is calculated and input into the formula for $D(z_i, \theta_i)$ derived by Schumaker et al. (2000) as implemented in the stand-alone code ACFCalculator (Gaalswyk et al. 2016). A total of 1.15 μs of additional simulations (192 ns per temperature and force field) were needed to compute the full diffusivity maps.

Results

Equilibrium Simulations

The L*n* peptides studied here via long simulation timescales (multi-μs) can be seen to transition spontaneously between surface aligned (S) and transmembrane inserted (TM) conformations (Fig. 1), similar to the results reported previously with simulations using the OPLS force field and united atom lipid parameters (Ulmschneider et al. 2010b, 2011a, b). However, these transitions require much higher temperatures to occur for CHARMM36; for example, L8 at 120 °C has 31 transitions/μs using the OPLS force field (Ulmschneider et al. 2011b) but only 5 transitions/μs using the C36 force field (Fig. 1). At least 120 °C is needed to accumulate sufficient switching events, and the dwell time of the peptides at this temperature is observed to be in the μs range, much longer than what was seen with OPLS. The kinetics can be accelerated by further heating, where—in contrast to the OPLS simulations—the CHARMM36 simulations are fully helical even at 150 °C. Peptides do not unfold, nor is the bilayer disrupted at this superheated temperature (Ulmschneider et al. 2009; Ulmschneider et al. 2010a), although the area per lipid increases significantly, ranging from ~65 Å^2 at 50 °C to as much as 85 Å^2 at elevated temperatures. For $T > 150$ °C, we saw some temporary breakage of a few backbone hydrogen bonds, so we used helical restraints as we are not interested in the CHARMM36 melting curve of polyleucine at extreme (unphysiological) temperatures, but solely in its rigid-body S to TM transition behavior.

Despite the greatly reduced kinetics of the simulations as compared to OPLS, the observed orientations of the peptides are exactly the same for the two force fields: there are four dominant states, two surface aligned and two transmembrane—one with the N-terminus in the upper leaflet, and one with the C-terminus in the upper leaflet. Other orientations are energetically highly unfavored. The only difference between the force fields is that peptides are embedded slightly more deeply in the S-state when using OPLS as compared to CHARMM36, which is likely related to differences between the united-atom (UA) and all-atom (AA) lipids used, respectively.

One of the surprising results of the OPLS simulations was the lack of a temperature dependence of the S → TM partitioning free energy, with $\Delta G_{S\rightarrow TM} = \text{const.}$, and $\Delta S_{S\rightarrow TM} = 0$ (Ulmschneider et al. 2011b). When we calculate $\Delta G_{S\rightarrow TM}$ here for CHARMM36, we observe the same lack of temperature dependence (Fig. 2). The result for L8 is $\Delta G_{S\rightarrow TM} \approx -0.9 \pm 0.2$ kcal/mol, independent of temperature, which is within roughly 0.6 kcal/mol of the OPLS value found previously ($\Delta G_{S\rightarrow TM} \approx -1.5 \pm 0.2$ kcal/mol) (Ulmschneider et al. 2011b). Thus, the two very different protein and lipid force fields agree surprisingly well. The simulation lengths of 5–7 μs allow for a sufficient number transitions for $T > 120$ °C, leading to fully converged free energy surfaces and excluding the possibility that insufficient sampling could play a role (Fig. 3).

Free-Energy Calculations

To determine the reliability of the long-time-scale equilibrium simulations in predicting the free energy difference

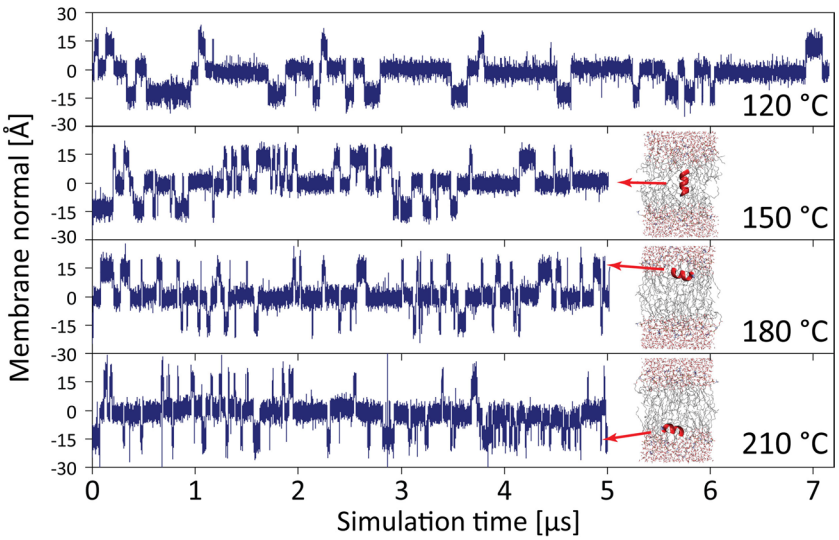

Fig. 1 The L8 peptide spontaneously switches between surface (S) and transmembrane (TM) states during equilibrium simulations using the CHARMM36 force field, shown here via plots of the center of mass position of the peptide along the membrane normal. The frequency of these switches increases rapidly with temperature. Very high temperature can be used without dissolving the membrane, and the peptides remain fully helical at 120 and 150 °C (for $T > 150$ °C, helical restraints were used). The kinetics are too slow for $T < 120$ °C to obtain convergence of $\Delta G_{S\rightarrow TM}$ on the simulated time scales

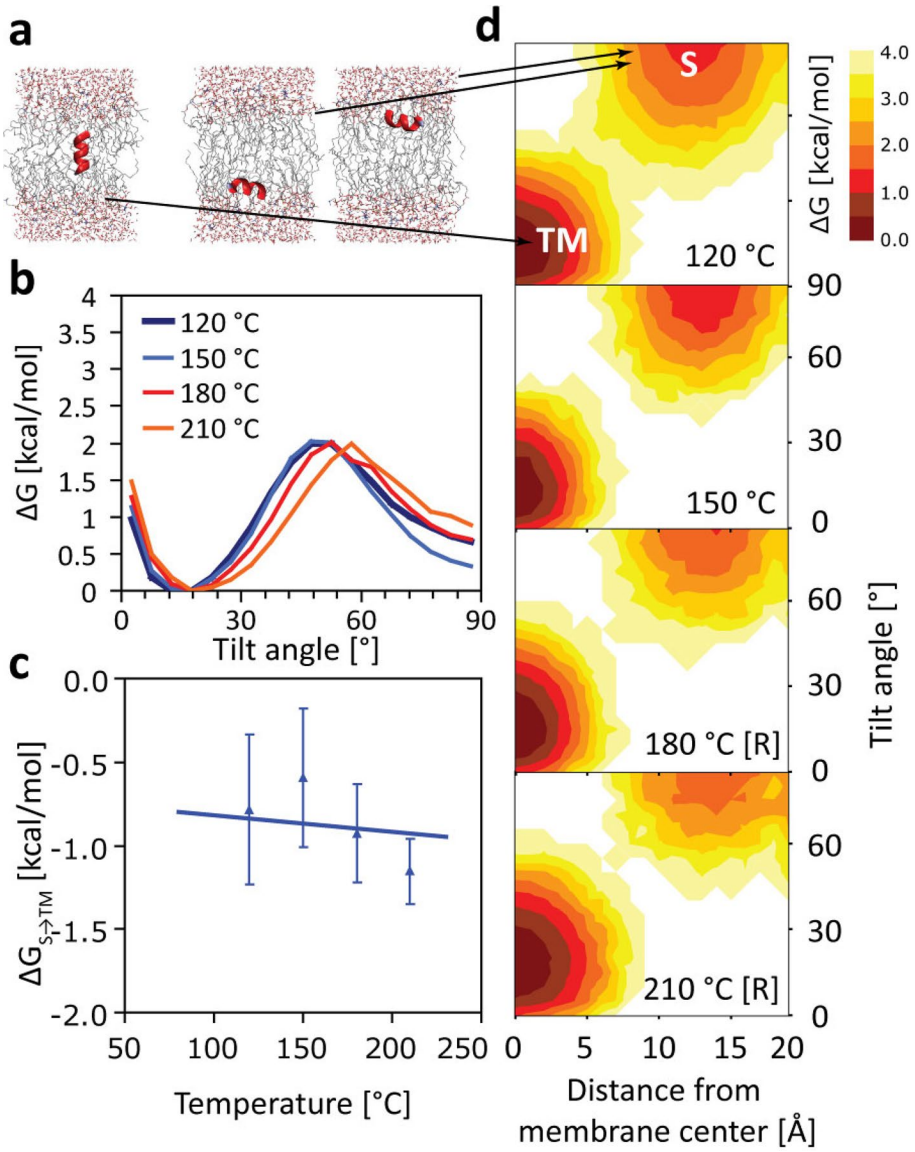

Fig. 2 **a** Temperature independence of hydrophobic S → TM partitioning for the L8 peptide in equilibrium simulations using the CHARMM36 force field. No pronounced temperature effect is visible over the range 120–210 °C. Each simulation plotted here is at least 5-μs long, so one-dimensional free energy profiles (**b**), and the overall transfer free energy $\Delta G_{S\rightarrow TM}$ (**c**), are well converged. Note that the barrier in **b** is not a true transition state, which is undersampled in our equilibrium simulations. Simulations using helical restraints are denoted with [R]. No unfolding is observed otherwise, and both unrestrained and restrained simulations yield the same $\Delta G_{S\rightarrow TM} \approx -0.9 \pm 0.2$ kcal/mol (**c**). Two-dimensional free energy profiles (as a function of membrane insertion and tilt angle) reveal almost no variation with temperature (**d**). (Color figure online)

between transmembrane and surface-associated states, we next turned to replica-exchange umbrella sampling (REMD-US). Two degrees of freedom relevant to the peptide were selected for biasing, the tilt angle of the helix and its position with respect to the membrane center. Potentials of mean force (PMFs) for both the CHARMM36 force field and the OPLS force field were determined at three temperatures each, 50, 120, and 160 °C. Each PMF calculation was run for 3 μs in total, with the exception of CHARMM36 at 50 °C, which was run for 3.8 μs (see "Methods").

The PMFs in Fig. 4 reveal the same general behavior observed for the equilibrium simulations in Fig. 2d, namely there are two preferred states (TM and S) with TM being slightly favored over S. To calculate $\Delta G_{S\rightarrow TM}$ for these two states, the 2D PMFs were integrated using Boltzmann weighting over the respective basins surrounding the two minima. With the exception of CHARMM36 at 50 °C, rough agreement between the PMF-derived $\Delta G_{S\rightarrow TM}$ values and the equilibrium values was found; for CHARMM36 above 50 °C, $\Delta G_{S\rightarrow TM}$ ranges from −1.4 to −1.3 kcal/mol, while for OPLS, the range is −1.6 to −1.0 kcal/mol (see Table 1). Thus, the transfer free energy of L8 is still found to be both force field and temperature independent (within less than 1 kcal/mol), at least above 50 °C. However, for CHARMM36 at 50 °C, $\Delta G_{S\rightarrow TM} = -2.86$ kcal/mol is much lower than the other values. There is little change, however, over time after the first few ns (see Fig. 3). Insufficient sampling (41 ns/window) of long-time-scale membrane rearrangements remains a possible issue, as the 10-μs simulation using CHARMM36 at 50 °C gives $\Delta G_{S\rightarrow TM} = -0.98$ kcal/mol, similar to the other calculations for L8. Indeed, sampling up to 205 ns/window was insufficient to determine accurately the free energy of binding of *n*-propylguanidinium

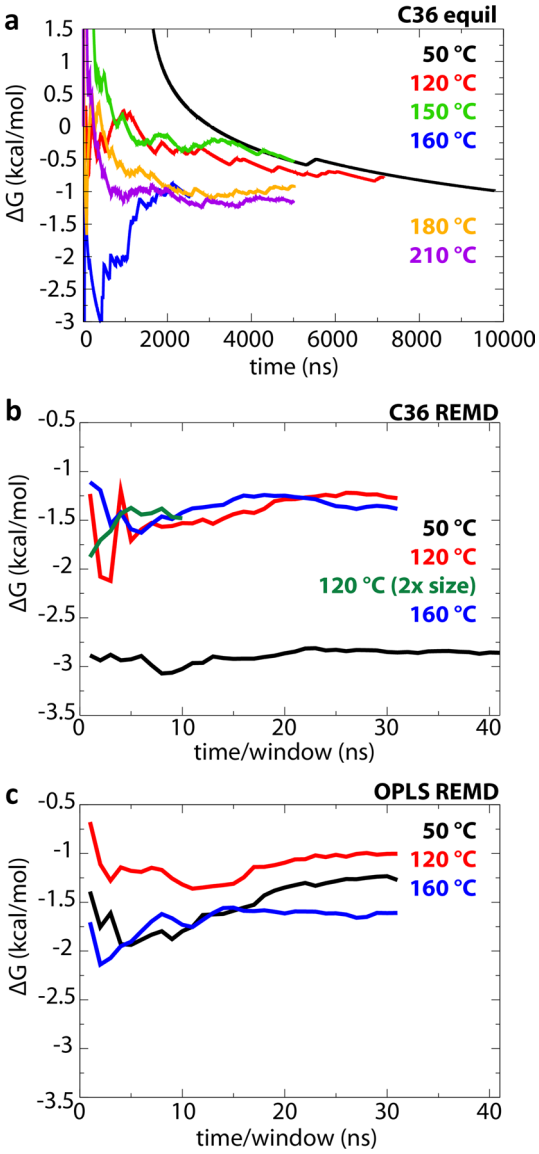

Fig. 3 Convergence of $\Delta G_{S\rightarrow TM}$. **a** $\Delta G_{S\rightarrow TM}$ as a function of time for all L8 equilibrium simulations. (**b**, **c**) $\Delta G_{S\rightarrow TM}$ as a function of sampling time per window for **b** CHARMM36 REMD calculations and **c** OPLS REMD calculations. (Color figure online)

to a DOPC bilayer, although the average of 36 independent calculations did converge to the expected result (Neale et al. 2011).

When the protein is in its S state, there is a difference in area/lipid between the two leaflets of the bilayer, one containing the protein and one not. This difference is either not present or not as pronounced for the TM state. Thus, finite-size effects may shift the free energies measured by adding a surface-tension-dependent term. To determine if such effects are manifest here, we repeated the REMD-US simulations for L8 in a bilayer of approximately twice the area as that used previously (91×91 Å^2 vs. 64×64 Å^2), using CHARMM36 and a temperature of 120 °C. Although run for a shorter time (1 μs vs. 3 μs), the resulting value of $\Delta G_{S\rightarrow TM}$ was almost identical to that found for the smaller membrane, − 1.5 kcal/mol versus − 1.3 kcal/mol, respectively. Thus, finite-size effects are not apparent here.

The similar transfer free energies for both the CHARMM36 and OPLS force fields, at least at temperatures above 50 °C, do not resolve the question of why the rate of transitions at equilibrium is significantly higher using OPLS over CHARMM36. To address this question, we calculated the least free energy path (LFEP) (Ensing et al. 2005) for each 2D PMF and extracted the activation energy. All cases exhibited a single barrier, indicating first-order kinetics. For OPLS, the TM → S activation energies are 6.2 kcal/mol at 50 °C (9.6 kT), 5.8 kcal/mol at 120 °C (7.5 kT), and 5.8 kcal/mol at 160 °C (6.7 kT). The activation energies found using CHARMM36 are almost identical for temperatures above 50 °C, namely 5.9 kcal/mol at 120 °C (7.5 kT) and 5.6 kcal/mol at 160 °C (6.5 kT).

Diffusivity Calculations

In addition to the size of the activation energy for transition between states, the kinetics of the process, specifically the diffusivity, also contributes to the rate of transitions. We calculated the diffusivity for both CHARMM36 and OPLS force fields at all three temperatures used for the REMD-US simulations, i.e., 50, 120, and 160 °C, plotted in Fig. 5. Diffusivity of the L8 peptide is consistently greater in the membrane than at the surface, where it is approximately two orders of magnitude less than in pure TIP3 water (Takemura and Kitao 2007). We also calculated the difference in diffusivities between OPLS/UA-lipids and CHARMM36/AA-lipids, as shown in Fig. 5g–i. The diffusivity in the membrane with UA-lipids is greater than that in AA-lipids for most orientations and positions of the L8 peptide. Although at $T=50$ °C, the difference between the two force fields is mixed, this difference grows with temperature. Greater diffusivity will lead to increased transition rates between states in OPLS/UA versus CHARMM36/AA, as observed in the equilibrium simulations described above.

The roughness of the energy landscape can have a significant effect on the diffusivity, with rougher landscapes resulting in slower dynamics due to the presence of small barriers along the reaction coordinate. This roughness is governed by the relation $D^*=D_0\exp[-(\varepsilon/kT)^2]$, where D_0 is the diffusion coefficient in a smooth potential, D^* is the diffusion coefficient in the true rough potential, ε is the roughness of the potential, k is Boltzmann's constant, and T is the temperature (Zwanzig 1988). This effect has been observed both computationally and experimentally. For example, in simulations of small peptides, explicit solvents increase the roughness of the torsional energy landscape by ~ 1.0 kcal/

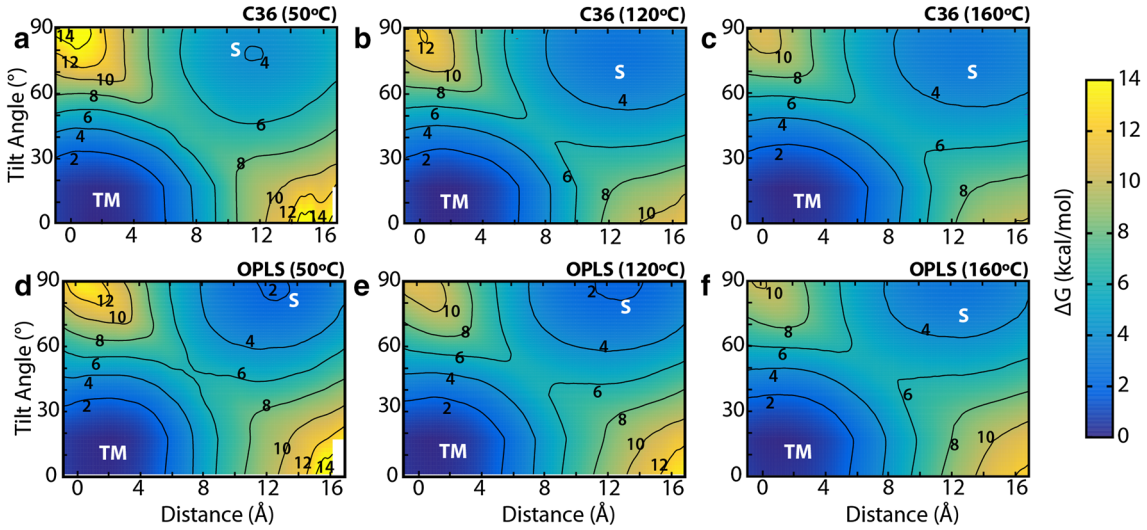

Fig. 4 Two-dimensional PMFs as a function of the L8 helix position along the membrane normal and its tilt angle. The transmembrane and surface-associated states are indicated by "TM" and "S." Contour lines are drawn every 2 kcal/mol and are labeled. (**a**–**c**) Plots for the CHARMM36 force field at **a** 50 °C, **b** 120 °C, and **c** 160 °C. (**d**–**f**) Plots for the OPLS force field at the same temperatures, respectively. (Color figure online)

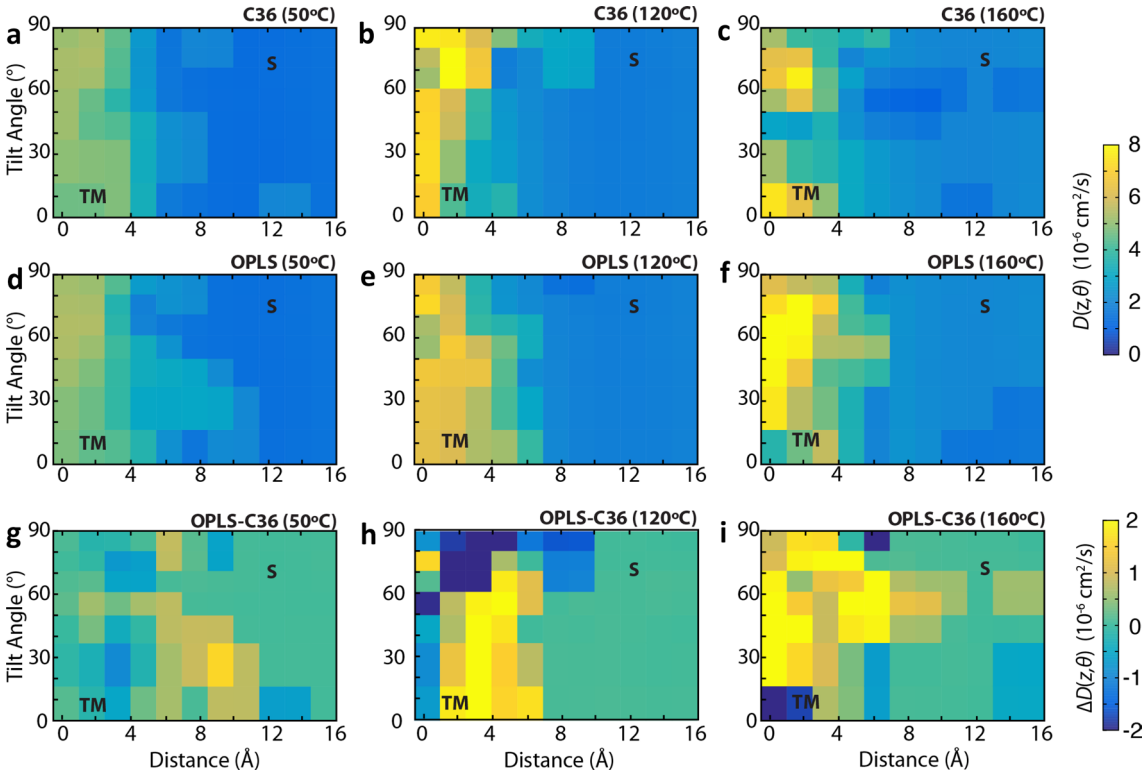

Fig. 5 Diffusivity as a function of position and tilt angle. **a**–**c** Diffusivity for CHARMM36 at **a** 50 °C, **b** 120 °C, and **c** 160 °C. **d**–**f** Diffusivity for OPLS at **d** 50 °C, **e** 120 °C, and **f** 160 °C. **g**–**i** The difference in diffusivities ($D^{\mathrm{OPLS}} - D^{\mathrm{C36}}$) at **g** 50 °C, **h** 120 °C, and **i** 160 °C. TM and S states are the same as indicated in Fig. 4. Values in **a**–**f** are colored on a scale of $0–8\times10^{-6}$ cm^2/s. (Color figure online)

mol over implicit solvents without affecting energy barriers or the location of local minima (Hamelberg et al. 2006). As a result, inter-residue ω-angle *cis*/*trans* isomerization rates were up to 10^4 times higher in the implicit solvent than the explicit solvent (Hamelberg et al. 2006). Changes in energetic roughness can also be critical mechanisms in biological

processes, such as the increase in roughness of the environment by ~ 1.0 kcal/mol as aminoacyl-tRNA transitions from free solution into the A-site of the ribosome, decreasing the diffusion constant by ~ 20× (Whitford et al. 2013). A similar phenomenon has also been observed in prion aggregation, where single-molecule force microscopy experiments have shown that dimerization of the prion protein, PrP, increases the energy landscape roughness by ~ 3.0 kcal/mol over the monomeric state, resulting in a 1000-fold decrease in the diffusion coefficient and 300-fold decrease in the unfolding rate for the misfolding pathway of the dimer versus the folding pathway of the monomer (Yu et al. 2015).

For united-atom lipid membranes, the lack of explicit hydrogens in the aliphatic tails should smooth the energy landscape, resulting in faster dynamics and more transitions of the helix than in all-atom lipid membranes. Transition rates in UA-lipid membranes are ~ 40× those in the AA-lipid membranes at 120 °C: 31 transitions in 1 μs (Ulmschneider et al. 2011b) versus 5 transitions in 7 μs (this work), respectively. Using Kramer's rate formula, given that the free energy landscapes are nearly identical between UA and AA lipids, diffusivity alone could explain the stark difference is transition rates. Since it is quite noisy (Fig. 5), we averaged the diffusivity in three distinct regions: the transmembrane region (TM), the surface-associated region (S), and the transition state region (TS) (see Fig. 6, top graph). Typically, to calculate energetic roughness, one computes a linear fit to $\log(D)$ versus $1/(kT)^2$ for each system, where the slope is equal to $-\varepsilon^2$ and the log has base e (Hamelberg et al. 2006). However, calculating diffusivity in membranes is notoriously prone to convergence issues. Diffusivities of solutes permeating through a lipid bilayer typically require μs to ms to converge (Neale et al. 2011), and autocorrelation functions may not decay fast enough, leading to an underestimation of the diffusion coefficients (Lee et al. 2016). Given that some of the windows in Fig. 5 may not be fully converged, fitting to the three temperatures may yield inaccurate results.

Instead of fitting, we can approximate the difference in roughness between UA- and AA-lipid membranes by assuming that the roughness of the UA-lipid membrane is negligible, i.e., that diffusion in the UA-lipid is essentially free diffusion. Although an implicit lipid membrane would better represent free diffusion as shown by Hamelberg et al. (2006), one would need to find such a model that produces the same free energy landscape as the AA-lipid force fields in order to calculate a true free diffusion constant. The UA-lipid force field is a good approximation of free diffusion in this case since it is the simplest model that reproduces the AA-lipid free energy landscape. Therefore, we approximate the roughness of the AA-lipid membrane

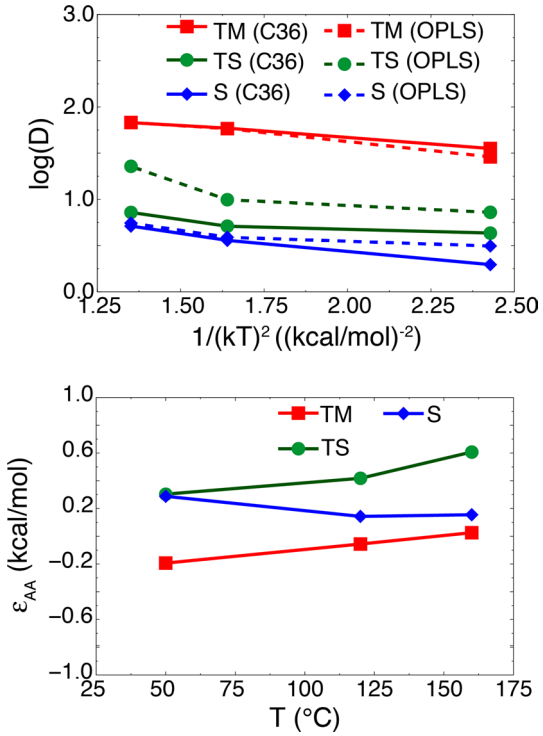

Fig. 6 Average diffusivities and energetic roughness. (Top) Average diffusivities for transmembrane ("TM," red curves), surface-associated ("S," blue curves), and transition ("TS," green) states for AA- (solid lines) and UA- (dashed lines) lipid membranes. TM and S states were defined as two potential wells observed in Fig. 4, with the TS state defined as the barrier region separating the two wells. Regions where the diffusivity calculations did not converge were excluded from the averages. Results are plotted as $\log(D)$ versus $1/(kT)^2$. (Bottom) Energetic roughness of AA-lipid membranes, approximated as $\varepsilon_{AA} \approx kT[\log(D_{UA}) - \log(D_{AA})]^{1/2}$, calculated for TM (red lines, squares), S (blue lines, diamonds), and TS (green lines, circles) states

at each temperature as $\varepsilon_{AA} \approx kT[\log(D_{UA}) - \log(D_{AA})]^{1/2}$ if $D_{UA} > D_{AA}$ or $-kT[\log(D_{AA}) - \log(D_{UA})]^{1/2}$ if $D_{UA} < D_{AA}$. These results are plotted in Fig. 6, bottom graph. At higher temperatures, the roughness of the transition-state (TS) region is ~ 0.4–0.6 kcal/mol in the AA-lipid membrane, whereas the roughness of the S and TM states is smaller (< 0.2 kcal/mol). Increased roughness in the transition-state region between the TM and S states may be driving the decrease in transition rates in the AA-lipid membrane, as was the case for prion misfolding (Yu et al. 2015). The roughness values also appear to be in line with the modest increase in transition rates between UA-lipid membranes and AA-lipid membranes; previous studies have found ~ 300×–10,000× for 1.0–3.0 kcal/mol (Hamelberg et al. 2006; Yu et al. 2015), whereas we only observe ~ 40× increase in transitions for 0.5 kcal/mol.

Ln Insertion Curve

We further calculated L5, L6, L7, L9, and L10 insertion using direct partitioning simulations at 150–210 °C, to complete a length scan for CHARMM36, similar to the one performed for OPLS before. The results are shown in Fig. 7. The insertion curve is very similar for both force fields (upper panel). The free energy can be reliably calculated for sequences with $|\Delta G_{S\rightarrow TM}| < 5$ kcal/mol (lower panel). The same linearity of $\Delta G_{S\rightarrow TM}$ with peptide length is found with the CHARMM36 parameters, albeit with a slightly larger slope of $\Delta\Delta G_{S\rightarrow TM} = -1.23$ kcal/mol, as compared to the OPLS value of $\Delta\Delta G_{S\rightarrow TM} = -0.91$ kcal/mol (Ulmschneider et al. 2011b). The similarity of two entirely different force fields is remarkable, and we believe that these values accurately represent the spontaneous insertion behavior of polyleucine in a lipid bilayer. The shift with respect to the translocon curve is due to the structural details of the translocon, where a different equilibrium is sampled.

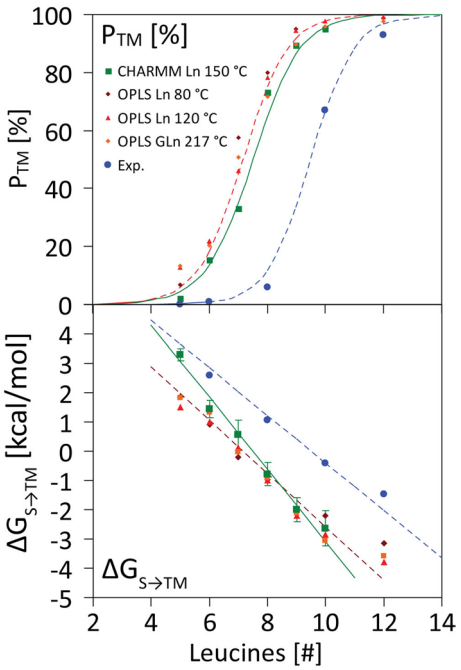

Fig. 7 Membrane insertion efficiency as a function of peptide length n for spontaneous partitioning of polyleucine (Ln) peptides into POPC lipid bilayers. (top) Insertion propensity. The computed values for the OPLS/UA-lipid force field at 80 and 120 °C (red) and GGPG-$(L)_n$-GPGG at 217 °C (brown) are shown. CHARMM36/AA-lipid results are also shown in the same figure (green). The results of the CHARMM36 simulations are very close to the OPLS results, and both show perfect two-state Boltzmann behavior ($R^2 > 0.99$), with a transition from a surface to TM state upon lengthening of the peptide. The experimental values are for translocon-mediated insertion into dog pancreas rough microsomes of GGPG-$(L)_n$-GPGG constructs embedded into the leader peptidase carrier sequence (Jaud et al. 2009). (bottom) Free energy of TM insertion from the surface $\Delta G_{S\rightarrow TM}$ as a function of peptide length n (insertion for negative ΔG). The straight lines indicate the two-state Boltzmann fit, while the data points show the computed (red, green) and experimental (blue) values for the individual peptides. (Color figure online)

Discussion

From the results of the simulations, one can conclude that (a) direct partitioning simulations and PMF calculations give similar results using roughly equivalent sampling effort, (b) hydrophobic peptide partitioning is independent of temperature and appears isentropic, (c) $\Delta G_{S\rightarrow TM}$ is independent of the force field used in the simulations, and (d) the kinetics of partitioning depends on the force field. This last observation appears to be due to the difference between UA-lipids and AA-lipids. UA-lipid tails have no charge and behave like a pure Lennard-Jones fluid, allowing for a smooth energy landscape for partitioning. In contrast, AA-lipid tails consist of small polar CH_2 groups, and the additional hydrogens generate a rougher energy landscape, as demonstrated by the roughness calculations above (Fig. 6). Given that the transition is isentropic and independent of the force field, the total enthalpic contribution to the free energy barrier, including protein–lipid, lipid–water, and protein-water interactions, must be similar. As it is highly unlikely that differences in all these interactions between the two force fields would exactly cancel each other out to produce a similar free energy, these interactions individually are probably similar as well. Therefore, the energetic roughness is likely the underlying factor for the observed differences in kinetics between the UA- and AA-lipid membranes.

With the exception of CHARMM36 REMD-US simulations at 50 °C, the net result of the simulations of L8 is that $\Delta G_{S\rightarrow TM} = -1.1 \pm 0.3$ kcal/mol, supporting the conclusion that $\Delta G_{S\rightarrow TM}$ is largely independent of the force field and temperature. The present work is also a demonstration that PMF calculations of peptides in lipid bilayers often agree with direct simulations if sufficient sampling is performed, which has previously been debated (Neale et al. 2011; Neale et al. 2014); albeit, both may yet suffer some unknown sampling deficiency, as suggested by the anomalous result for CHARMM36 REMD-US simulations at 50 °C. As noted before (Ulmschneider et al. 2011b, 2014), there is a shift between the spontaneous insertion and the translocon-based scale (Hessa et al. 2007), with the latter being ~2 kcal/mol higher (less favorable). This shift can be explained in part by structural details of the translocon, which is apparently less polar than a purely aqueous environment (Capponi et al. 2015; Bol et al. 2007; Demirci et al. 2013; Gumbart et al. 2011a), and possibly also by the kinetics of the biological insertion process (Gumbart and Chipot 2016; Gumbart et al. 2013; Zhang and Miller III, 2012b). Regardless of the precise origins, we have

demonstrated here that errors in the simulation protocol are not responsible for the distinct energies found for the two processes. Furthermore, our results provide additional evidence that the energies measured in the translocon-based experiments do not represent an equilibrium partitioning between water and membrane, but something more complex (Cymer et al. 2015; Gumbart et al. 2011b; Schow et al. 2011).

The equivalence of the calculated free energies using both two distinct force fields and two disparate methods imparts a degree of confidence in the quantitative accuracy of MD simulations, at least for the energetics of protein-lipid interactions. While it may be claimed that both force fields, CHARMM36/AA and OPLS/UA, are producing identical differences from the translocon-based scale, such a coincidence seems unlikely. However, the importance of reaching convergence in the measured properties cannot be understated, and membranes in particular can be slow to equilibrate (Neale et al. 2011). Nonetheless, the results presented here demonstrate the utility of MD simulations for studying other spontaneous-insertion processes applicable to, e.g., the design of novel antimicrobial peptides.

Acknowledgements J. C. G. acknowledges funding support from NSF (MCB-1452464) and NIH (R01-GM123169) and S. H. W acknowledges NIH support (RO1-GM74639). J. P. U. was supported by a China 1000 Plan's Program for Young Talents (13Z127060001). Simulation resources were provided by the Center for High Performance Computing, Shanghai Jiao Tong University and the Maryland Advanced Research Computing Center (MARCC). This work used the Extreme Science and Engineering Discovery Environment (XSEDE), which is supported by National Science Foundation grant number ACI-1548562. Anton computer time was provided by the Pittsburgh Supercomputing Center (PSC) through Grant R01GM116961 from the National Institutes of Health. The Anton machine at PSC was generously made available by D. E. Shaw Research.

Compliance with Ethical Standards

Conflict of interest All authors declare they have no conflict of interest.

Ethical Approval This article does not contain any studies with human participants or animals performed by any of the authors.

References

Babakhani A, Gorfe AA, Kim JE, McCammon JA (2008) Thermodynamics of peptide insertion and aggregation in a lipid bilayer. J Phys Chem B 112:10528–10534

Bechinger B (1997) Structure and functions of channel-forming peptides: magainins, cecropins, melittin and alamethicin. J Membr Biol 156:197–211

Berendsen HJC, Postma JPM, Vangunsteren WF, Dinola A, Haak JR (1984) Molecular-dynamics with coupling to an external bath. J Chem Phys 81:3684–3690

Berendsen HJC, van der Spoel D, van Drunen R (1995) GROMACS: a message-passing parallel molecular dynamics implementation. Comput Phys Commun 95:43–56

Best RB, Zhu X, Shim J, Lopes PE, Mittal J, Feig M, MacKerell AD Jr (2012) Optimization of the additive CHARMM all-atom protein force field targeting improved sampling of the backbone φ, ψ and side-chain χ_1 and χ_2 dihedral angles. J Chem Theory Comput 8:3257–3273

Bol R, de Wit JG, Driessen AJM (2007) The active protein-conducting channel of *Escherichia coli* contains an apolar patch. J Biol Chem 282:29785–29793

Bussi G, Donadio D, Parrinello M (2007) Canonical sampling through velocity rescaling. J Chem Phys 126:014101

Capponi S, Heyden M, Bondar A-N, Tobias DJ, White SH (2015) Anomalous behavior of water inside the SecY translocon. Proc Natl Acad Sci 112:9016–9021

Cymer F, von Heijne G, White SH (2015) Mechanisms of integral membrane protein insertion and folding. J Mol Biol 427:999–1022

Demirci E, Junne T, Baday S, Bernèche S, Spiess M (2013) Functional asymmetry within the Sec61p translocon. Proc Natl Acad Sci USA 110:18856–18861

Dorairaj S, Allen TW (2007) On the thermodynamic stability of a charged arginine side chain in a transmembrane helix. Proc Natl Acad Sci USA 104:4943–4948

Ensing B, Laio A, Parrinello M, Klein ML (2005) A recipe for the computation of the free energy barrier and the lowest free energy path of concerted reactions. J Phys Chem B 109:6676–6687

Feller SE, Zhang YH, Pastor RW, Brooks BR (1995) Constant pressure molecular dynamics simulations—the Langevin piston method. JCP 103:4613–4621

Frauenfeld J, Gumbart J, Sluis EO, Funes S, Gartmann M, Beatrix B, Mielke T, Berninghausen O, Becker T, Schulten K, Beckmann R (2011) Cryo-EM structure of the ribosome-SecYE complex in the membrane environment. Nat Struct Mol Biol 18:614–621

Gaalswyk K, Awoonor-Williams E, Rowley CN (2016) Generalized Langevin methods for calculating transmembrane diffusivity. J Chem Theory Comput 12:5609–5619

Gumbart J, Chipot C, Schulten K (2011a) Free energy of nascent-chain folding in the translocon. J Am Chem Soc 133:7602–7607

Gumbart J, Chipot C, Schulten K (2011b) Free-energy cost for translocon-assisted insertion of membrane proteins. Proc Natl Acad Sci USA 108:3596–3601

Gumbart J, Roux B (2012) Determination of membrane-insertion free energies by molecular dynamics simulations. Biophys J 102:795–801

Gumbart JC, Chipot C (2016) Decrypting protein insertion through the translocon with free-energy calculations. Biochim Biophys Acta 1858:1663–1671

Gumbart JC, Teo I, Roux B, Schulten K (2013) Reconciling the roles of kinetic and thermodynamic factors in membrane–protein insertion. J Am Chem Soc 135:2291–2297

Hamelberg D, Shen T, McCammon AJ (2006) Insight into the role of hydration on protein dynamics. J Chem Phys 125:094905

Hess B, Bekker H, Berendsen HJC, Fraaije JGEM. (1997) LINCS: a linear constraint solver for molecular simulations. J Comput Chem 18:1463–1472

Hessa T, Kim H, Bihlmaier K, Lundin C, Boekel J, Andersson H, White SH, von Heijne G (2005) Recognition of transmembrane helices by the endoplasmic reticulum translocon. Nature 433:377–381

Hessa T, Meindl-Beinker NM, Bernsel A, Kim H, Sato Y, Lerch-Bader M, Nilsson I, White SH, von Heijne G (2007) Molecular code for transmembrane-helix recognition by the Sec61 translocon. Nature 450:1026–1030

Hoover WG (1985) Canonical dynamics: equilibrium phase-space distributions. Phys Rev A 31:1695–1697

Horn JN, Romo TD, Grossfield A (2013) Simulating the mechanism of antimicrobial lipopeptides with all-atom molecular dynamics. Biochemistry 52:5604–5610

Hu X, Hong L, Smith MD, Neusius T, Cheng X, Smith JC (2016) The dynamics of single protein molecules is non-equilibrium and self-similar over thirteen decades in time. Nat Phys 12:171–174

Humphrey W, Dalke A, Schulten K (1996) VMD—visual molecular dynamics. J Mol Gr 14:33–38

Irudayam SJ, Pobandt T, Berkowitz ML (2013) Free energy barrier for melittin reorientation from a membrane-bound state to a transmembrane state. J Phys Chem B 117:13457–13463

Jaud S, Fernández-Vidal M, Nillson I, Meindl-Beinker NM, Hübner NC, Tobias DJ, von Heijne G, White SH (2009) Insertion of short transmembrane helices by the Sec61 translocon. Proc Natl Acad Sci USA 106:11588–11593

Johansson ACV, Lindahl E (2008). Position-resolved free energy of solvation for amino acids in lipid membranes from molecular dynamics simulations. Proteins Struct Funct Genet 70:1332–1344

Jorgensen WL, Chandrasekhar J, Madura JD, Impey RW, Klein ML (1983) Comparison of simple potential functions for simulating liquid water. J Chem Phys 79:926–935

Jorgensen WL, Maxwell DS, Tirado-Rives J (1996) Development and testing of the OPLS all-atom force field on conformational energetics and properties of organic liquids. J Am Chem Soc 118:11225–11236

Klauda JB, Venable RM, Freites JA, O'Connor JW, Tobias DJ, Mondragon-Ramirez C, Vorobyov I, MacKerell AD Jr, Pastor RW (2010) Update of the CHARMM all-atom additive force field for lipids: validation on six lipid types. J Phys Chem B 114:7830–7843

Ladokhin AS, White SH (1999) Folding of amphipathic α-helices on membranes: energetics of helix formation by melittin. J Mol Biol 285:1363–1369

Ladokhin AS, White SH (2004) Interfacial folding and membrane insertion of a designed helical peptide. Biochemistry 43:5782–5791

Lee C, Comer J, Herndon C, Leung N, Pavlova A, Swift R, Tung C, Rowley C, Amaro R, Chipot C, Wang Y, Gumbart JC (2016) Simulation-based approaches for determining membrane permeability of small compounds. J Chem Inf Model 56:721–733

Lippert RA, Predescu C, Ierardi DJ, Mackenzie KM, Eastwood MP, Dror RO, Shaw DE (2013) Accurate and efficient integration for molecular dynamics simulations at constant temperature and pressure. J Chem Phys 139:164106

Lyu Y, Xiang N, Zhu X, Narsimhan G (2017) Potential of mean force for insertion of antimicrobial peptide melittin into a pore in mixed DOPC/DOPG lipid bilayer by molecular dynamics simulation. J Chem Phys 146:155101

MacCallum JL, Bennett WFD, Tieleman DP (2007) Partitioning of amino acid side chains into lipid bilayers: results from computer simulations and comparison to experiment. J Gen Physiol 129:371–377

Martyna GJ, Klein ML, Tuckerman M (1992) Nosé-Hoover chains—the canonical ensemble via continuous dynamics. J Chem Phys 97:2635–2643

Martyna GJ, Tobias DJ, Klein ML (1994) Constant pressure molecular dynamics algorithms. J Chem Phys 101:4177–4189

Moon CP, Fleming KG (2011) Side-chain hydrophobicity scale derived from transmembrane protein folding into lipid bilayers. Proc Natl Acad Sci USA 108:10174–10177

Neale C, Bennett WFD, Tieleman DP, Pomès R (2011) Statistical convergence of equilibrium properties in simulations of molecular solutes embedded in lipid bilayers. J Chem Theory Comput 7:4175–4188

Neale C, Hsu JC, Yip CM, Pomès R (2014) Indolicidin binding induces thinning of a lipid bilayer. Biophys J 106:L29–L31

Park E, Ménétret J-F, Gumbart JC, Ludtke SJ, Li W, Whynot A, Rapoport TA, Akey CW (2014) Structure of the SecY channel during initiation of protein translocation. Nature 506:102–106

Phillips JC, Braun R, Wang W, Gumbart J, Tajkhorshid E, Villa E, Chipot C, Skeel D, Kale R, Schulten L, K (2005) Scalable molecular dynamics with NAMD. J Comput Chem 26:1781–1802

Piggot TJ, Piñeiro A, Khalid S (2012) Molecular dynamics simulations of phosphatidylcholine membranes: a comparative force field study. J Chem Theory Comput 8:4593–4609

Sandoval-Perez A, Pluhackova K, Bockmann RA (2017) Critical comparison of biomembrane force fields: protein-lipid interactions at the membrane interface. J Chem Theory Comput 13:2310–2321

Sato H, Feix JB (2006) Peptide–membrane interactions and mechanisms of membrane destruction by amphipathic α-helical antimicrobial peptides. Biochim Biophys Acta 1758:1245–1256

Schlamadinger DE, Wang Y, McCammon JA, Kim JE (2012) Spectroscopic and computational study of melittin, cecropin A, and the hybrid peptide CM15. J Phys Chem B 116:10600–10608

Schow EV, Freites JA, Cheng P, Bernsel A, von Heijne G, White SH, Tobias DJ (2011) Arginine in membranes: the connection between molecular dynamics simulations and translocon-mediated insertion experiments. J Membr Biol 239:35–48

Schumaker M, Pomès R, Roux B (2000) A combined molecular dynamics and diffusion model of single proton conduction through gramicidin. Biophys J 79:2840–2857

Shaw DE, Dror RO, Salmon JK, Grossman JP, Mackenzie KM, Bank JA, Young C, Deneroff MM, Batson B, Bowers KJ, Chow E, Eastwood MP, Ierardi DJ, Klepeis JL, Kuskin JS, Larson RH, Lindorff-Larsen K, Maragakis P, Moraes MA, Piana S, Shan Y, Towles B (2009). Millisecond-scale molecular dynamics simulations on Anton. ACM/IEEE conference on supercomputing (SC09). ACM Press, Portland

Sugita Y, Kitao A, Okamoto Y (2000) Multidimensional replica-exchange method for free-energy calculations. J Chem Phys 113:6042–6051

Takemura K, Kitao A (2007) Effects of water model and simulation box size on protein diffusional motions. J Phys Chem B 111:11870–11872

Ulmschneider JP (2017) Highly charged antimicrobial peptides can permeabilize and translocate across lipid bilayers without forming channel-like pores. Biophys J 113:73–81

Ulmschneider JP, Andersson M, Ulmschneider MB (2011a) Determining peptide partitioning properties via computer simulation. J Membr Biol 239:15–26

Ulmschneider JP, Doux JPF, Killian JA, Smith JC, Ulmschneider MB (2009) Peptide partitioning and folding into lipid bilayers. J Chem Theor Comput 5:2202–2205

Ulmschneider JP, Smith JC, White SH, Ulmschneider MB (2011b) In silico partitioning and transmembrane insertion of hydrophobic peptides under equilibrium conditions. J Am Chem Soc 133:15487–15495

Ulmschneider MB, Doux JPF, Killian JA, Smith JC, Ulmschneider JP (2010a) Mechanism and kinetics of peptide partitioning into membranes from all-atom simulations of thermostable peptides. J Am Chem Soc 132:3452–3460

Ulmschneider MB, Smith JC, Ulmschneider JP (2010b) Peptide partitioning properties from direct insertion studies. Biophys J 98:L60–L62

Ulmschneider MB, Ulmschneider JP, Schiller N, Wallace BA, von Heijne G, White SH (2014) Spontaneous transmembrane helix insertion thermodynamically mimics translocon-guided insertion. Nat Commun 5:4863

Upadhyay S, Wang Y, Zhao T, Ulmschneider JP (2015) Insights from micro-second atomistic simulations of melittin in thin lipid bilayers. J Membr Biol 248:497–503

van den Berg B, Clemons WM Jr, Collinson I, Modis Y, Hartmann E, Harrison SC, Rapoport TA (2004) X-ray structure of a protein-conducting channel. Nature 427:36–44

Wang Y, Chen CH, Hu D, Ulmschneider MB, Ulmschneider JP (2016) Spontaneous formation of structurally diverse membrane channel architectures from a single antimicrobial peptide. Nat Commun 7:13535

Whitford PC, Blanchard SC, Cate JHD, Sanbonmatsu KY (2013) Connecting the kinetics and energy landscape of tRNA translocation on the ribosome. PLoS Comput Biol 9:e1003003

Wimley WC, White SH (2000) Designing transmembrane α-helices that insert spontaneously. Biochemistry 39:4432–4442

Yeh I-C, Olson MA, Lee MS, Wallqvist A (2008) Free-energy profiles of membrane insertion of the M2 transmembrane peptide from influenza A Virus. Biophys J 95:5021–5029

Yu H, Dee DR, Liu X, Brigley AM, Sosova I, Woodside MT (2015) Protein misfolding occurs by slow diffusion across multiple barriers in a rough energy landscape. Proc Natl Acad Sci USA 112:8308–8313

Zhang B, Miller TF, III (2012a). Direct simulation of early-stage sec-facilitated protein translocation. J Am Chem Soc. 134:13700–13707

Zhang B, Miller TF, III (2012b). Long-timescale dynamics and regulation of sec-facilitated protein translocation. Cell Rep 2:927–937

Zwanzig R (1988) Diffusion in a rough potential. Proc Natl Acad Sci USA 85:2029–2030